Petroleum 3 (2017) 96–108

Contents lists available at ScienceDirect

Petroleum

journal homepage: www.keaipublishing.com/en/journals/petlm

Change in cap rock porosity triggered by pressure and temperature dependent CO_2–water–rock interactions in CO_2 storage systems

Christina Hemme*, Wolfgang van Berk

TU Clausthal, Institute of Disposal Research, Department of Hydrogeology, Leibnizstrasse 10, 38642 Clausthal-Zellerfeld, Germany

ARTICLE INFO

Article history:
Received 27 June 2016
Received in revised form
3 November 2016
Accepted 9 November 2016

ABSTRACT

Carbon capture and storage in deep geological formations is a method to reduce greenhouse gas emissions. Supercritical CO_2 is injected into a reservoir and dissolves in the brine. Under the impact of pressure and temperature (P–T) the aqueous species of the CO_2-acidified brine diffuse through the cap rock where they trigger CO_2–water–rock interactions. These geochemical reactions result in mineral dissolution and precipitation along the CO_2 migration path and are responsible for a change in porosity and therefore for the sealing capacity of the cap rock. This study focuses on the diffusive mass transport of CO_2 along a gradient of decreasing P–T conditions. The process is retraced with a one-dimensional hydrogeochemical reactive mass transport model. The semi-generic hydrogeochemical model is based on chemical equilibrium thermodynamics. Based on a broad variety of scenarios, including different initial mineralogical, chemical and physical parameters, the hydrogeochemical parameters that are most sensitive for safe long-term CO_2 storage are identified. The results demonstrate that P–T conditions have the strongest effect on the change in porosity and the effect of both is stronger at high P–T conditions because the solubility of the mineral phases involved depends on P–T conditions. Furthermore, modeling results indicate that the change in porosity depends strongly on the initial mineralogical composition of the reservoir and cap rock as well as on the brine compositions. Nevertheless, a wide range of conditions for safe CO_2 storage is identified.

1. Introduction and aim

A solution to reduce CO_2 emissions into the atmosphere is the storage of CO_2 in the reservoir rocks of depleted hydrocarbon reservoirs, coal seams and deep saline aquifers [1]. For the storage of CO_2 four different trapping mechanisms are known: (1) structural trapping, (2) residual trapping, (3) dissolution trapping, and (4) mineral trapping [2,3]. Black et al. [4] stated that the effects of mineral dissolution and precipitation are the key factors for safe CO_2 storage. The injection of CO_2 leads to CO_2–water–rock interactions that result in the precipitation and dissolution of minerals which in turn result in a change in porosity and permeability of the cap rock. This change leads to the improvement or deterioration of the sealing capacity of the cap rock. Mineral dissolution results in an increase in porosity and enables the creation of pathways for CO_2 migration. Mineral precipitation leads to a decrease in porosity and increases the sealing effect [5]. In the discussion about carbon capture and storage (CCS) many studies focus on CO_2-water-rock interactions in reservoir rocks but much less attention has been paid on these interactions in the cap rock. Consequently, forecasting and quantifying such CO_2–induced processes in cap rocks rank high on the agenda for successful carbon capture and storage in deep geological formations. Thus, various modeling and experimental

* Corresponding author.
E-mail addresses: christina.hemme@tu-clausthal.de (C. Hemme), wolfgang.van.berk@tu-clausthal.de (W. van Berk).

Peer review under responsibility of Southwest Petroleum University.

Production and Hosting by Elsevier on behalf of KeAi

http://dx.doi.org/10.1016/j.petlm.2016.11.010

studies aim to retrace and reproduce such hydrogeochemical reactions in cap rocks [4–15].

Knowledge of cap rock properties is important for these studies. Cap rocks are characterized by specific mineralogical and physical properties like low porosity and permeability. The often clay-bearing cap rocks have to be saturated with brine and must have a capillary entry pressure that prevents the cap rock from supercritical CO_2 entering [16] and prevents CO_2 from escaping towards overlying aquifers needed for water supply [17].

Our study is based on equilibrium thermodynamics of chemical CO_2–water–rock interactions to fundamentally reveal where a carbon capture and storage system inevitably develops in terms of porosity alteration resulting from mineral dissolution and precipitation. It is not our aim to reproduce a real complex geological system. Correspondingly, our modeling approach is of semi-generic nature. We aim to identify long-term inorganic hydrogeochemical processes including CO_2–water–rock interactions and to quantify the change in porosity due to the effects of geochemical reactions in dependence on pressure and temperature. This process is retraced with a one-dimensional hydrogeochemical reactive mass transport model based on a hypothetical concept. Authors like Bildstein et al. [10] have modeled porosity creation in the cap rock at constant temperature and pressure conditions. Generally, temperature and pressure conditions change along the path of diffusive transport of CO_2 [18] and could strongly affect the mass-action law constants for the equilibrium reactions between mineral phases and CO_2. Therefore, it is important to consider not only different temperature and pressure conditions at the starting point of diffusive CO_2 migration, like those modeled by Van Pham et al. [19], but also the change of temperature and pressure along the diffusive pathway of CO_2 through the cap rock. Therefore, this study will focus on the diffusive mass transport of CO_2 along a gradient of decreasing pressure and temperature conditions. A broad variety of modeling scenarios, including different initial mineralogical and physical parameters, is calculated to identify the hydrogeochemical parameters most sensitive for safe CO_2 storage. In addition, the numerical accuracy of our model is tested by a detailed grid convergence study.

2. Kinetic or thermodynamic equilibrium modeling for long-term CO_2 storage?

Various modeling studies related to cap rocks in CCS systems apply batch and/or reactive transport modeling approaches that include reaction kinetics [5,15,16]. These studies focus on the time-dependent progress of mineral dissolution and precipitation reactions which are characterized by associated reaction rate constants. An overview over the rate parameters of water-mineral interaction kinetics are given in a report by the U.S. Geological Survey [20]. Kinetic simulations still show uncertainties regarding the poor knowledge of the kinetic rate constants at elevated levels of temperature, total and CO_2 partial-pressure. However, such knowledge is essential for kinetically based modeling of CCS systems, especially in this study which focuses on the diffusive mass transport of CO_2 along a gradient of decreasing P–T conditions. In addition, the rates obtained in laboratory strongly depend on the experimental devices and the chosen boundary or environmental conditions, and therefore they are difficult to compare with another [21]. Ignoring the facts that i) hydrogeochemical conditions (e.g., pH, pε, ionic strength) evolve and change in time and space and ii) that kinetic rate constants must change accordingly, makes the modeling results meaningless –especially when thermodynamically impossible reactions are modeled.

Approaches based on kinetics start from the assumption that kinetically characterized reactions actually proceed –whether any driving force in terms of system thermodynamics allows these reactions to proceed or not. In contrast, thermodynamically based modeling approaches only calculate the reactions, which are thermodynamically possible, until spontaneous equilibrium conditions are established. The term spontaneous implies that the equilibrium is established for the residence time of CO_2 in a spatially discrete compartment. Stumm and Morgan [22] argued that applying thermodynamically based approaches allow to "identify reactions that are possible". In consequence, the authors developed "first equilibrium and then kinetic frameworks for natural water systems". Moreover, Marini [21] stated that equilibrium thermodynamics seem to be a good modeling tool for the analysis of chemical reactions in CO_2 storage systems. This appraisal is based on the studies performed by Helgeson [23–27] which show that a separation of the overall reaction path into a series of partial equilibrium states enables successful modeling based on chemical equilibrium thermodynamics.

One of the main differences between thermodynamically based modeling studies and approaches including reaction kinetics [5,15,16] is the total time considered by the modeling of specific reactive transport processes. In their kinetically based modeling study, Mohd Amin et al. [16] considered a total time of 10,000 years referring to the fact that Bowden and Rigg [28] and Credoz et al. [6] asserted that such a timescale is relevant for the long-term safety assessment of CO_2 storage. However, this determination of Bowden and Rigg [28] and Credoz et al. [6] is presented without any retraceable justification. Tian et al. [15] performed all their simulations considering a total time of 1000 years while Gaus et al. [5] considered 15,000 years. Gaus et al. [5] concluded that when using kinetically based calculations the system is still far from equilibrium after 15,000 years. However and in contrast, to justify a relevant timescale our study calculates the diffusive transport of a non-reactive tracer through the model system for various total times and time step lengths –prior to any reactive transport modeling (for details, see Section 4.1.). From the time-dependent spatial spreading of this tracer we conclude that a total time of 1,000,000 years is the timescale relevant for the long-term safety assessment of CO_2 storage systems similar to our semi-generic modeling systems.

Considering these facts, we decide to perform modeling based on thermodynamics, although we are aware that the progress of various heterogeneous reactions is actually controlled by kinetics. It is not our aim to connect thermodynamically driven hydrogeochemical processes with temporal aspects. Our aim is to identify and quantify the long-term hydrogeochemical processes. Provided that thermodynamic equilibrium is established, the thermodynamically based modeling approach enables us to test where the CCS system is inevitably going in terms of porosity alteration.

3. Conceptual numerical model and modeling parameters

3.1. Model setup

The hydrogeochemical, one-dimensional reactive mass transport (1DRMT) modeling approach presented in this study is based on a semi-generic concept. It includes available data from several real CO_2 storage systems and is based on assumptions regarding non-available data for the sake of simplicity. Alternative scenarios for selected parameters are performed to reveal how strongly the parameters affect the CO_2–water–rock interactions (for details, see Section 5.2.).

The geological structure in this model is a depleted hydrocarbon reservoir in an anticlinal fold (Fig. 1.). Carbon dioxide is injected into the reservoir rock at a depth of about 800 m. At this depth CO_2 is supercritical ($CO_{2(sc)}$) and dissolves until the reservoir brine is saturated with respect to $CO_{2(aq)}$. The critical point for CO_2 lies at a temperature of 304.21 K (31.06 °C) and at a pressure of 73.825 bars (72.859 atm) according to Angus et al. [29] and Salimi et al. [30]. At temperature and pressure conditions above this critical point, the $CO_{2(sc)}$ is present in a dense phase which is lighter than the brine in the reservoir rock and migrates from the point of injection to the reservoir/cap rock contact where a $CO_{2(sc)}$ plume builds up (Fig. 1.) [31]. During this process the reservoir brine is displaced by the supercritical $CO_{2(sc)}$. At the contact with the cap rock CO_2 is available as $CO_{2(sc)}$ in the plume and as dissolved CO_2 ($CO_{2(aq)}$ and corresponding aqueous species e.g. HCO_3^-, CO_3^{2-}, $CaHCO_3^+$, H^+) in the reservoir brine beneath the plume. The $CO_{2(sc)}$ dissolves in the cap rock brine and an acidic solution is created. Molecular diffusion of aqueous species through the cap rock brine leads to $CO_{2(aq)}$–water–rock interactions in the cap rock that cause mineral dissolution and precipitation and therefore a change in the porosity and permeability of the cap rock. The mass-action law constants for the equilibrium reactions between mineral phases and $CO_{2(aq)}$ depend on temperature and pressure, and therefore they change along the $CO_{2(aq)}$ migration path [18].

Our hydrogeochemical model is based on thermodynamic equilibrium reactions and the local equilibrium assumption. Kinetic aspects of mineral dissolution/precipitation are not considered. Even if CO_2 is supercritical under the assumed reservoir conditions, this model uses gaseous CO_2 as an analog. This simplifying assumption is based on the study of Rochelle and Moore [32] that shows results of supercritical CO_2 solubility experiments at different pressure and temperature conditions. We retraced these experiments using PHREEQC Interactive 3.1.4–8929 and its database phreeqc.dat, with the difference that we used gaseous CO_2 instead of supercritical CO_2. The solubility constants for $CO_{2(g)}$ used in PHREEQC and $CO_{2(sc)}$ measured by Rochelle and Moore [32] are similar and consequently the following reactions apply:

$$CO_{2(g)} = CO_{2(aq)} \log K = -1.468; \text{ at } 25\ ^\circ C; 1 \text{ bar} \quad (1)$$

$$CO_{2(sc)} = CO_{2(aq)} \log K = -1.468; \text{ at } 25\ ^\circ C; 1 \text{ bar} \quad (2)$$

Furthermore, to prove and quantify this assumption a separate sensitivity analysis is presented in Section 5.3.

In the model the migration path is demonstrated by a column of 101 cells, with a cell length of 1 m. One cell is located in the reservoir rock and one hundred cells are located in the cap rock (Fig. 1.). For both ends of the column the modeling boundary conditions are defined as flux. Due to a constant ρCO_2 in the plume, the lower boundary can be interpreted as a constant concentration boundary. By adding five extra cells at the upper end of the column, the influence of the upper boundary condition can be minimized, considering that only the 101 cells are evaluated. The only mass transport mechanism in this model is molecular diffusion of all aqueous species through the cap rock brine. The process of diffusion of aqueous species is slow [5] but allows the mass transport of dissolved species between all cells [33], depending on time and diffusivity. One diffusion coefficient for all aqueous species of 3.33×10^{-10} m^2/s is used. This value is based on the assumption made by Mohd Amin et al. [16] that the diffusion coefficient is made up of the diffusion coefficient in pure water of 1×10^{-9} m^2/s divided by an averaging tortuosity of 3 [34].

3.2. Initial pressure and temperature conditions

The pressure and temperature conditions (P–T conditions) are similar to the conditions predominating at the CCS storage system at Sleipner in Norway, starting with 40.0 °C (37.0 °C at Sleipner) and 100.0 atm at reservoir conditions (100.0 atm at Sleipner). The temperature decreases from the reservoir depth up along the geothermal gradient, at 33.3 °C per kilometer of depth, and the pressure decreases accordingly with 100.0 atm per kilometer under hydrostatic conditions. Consequently, each of the 101 cells is associated with a specific pressure/temperature condition (for example, cell 1: 40.0 °C and 100.0 atm, cell 2: 39.967 °C and 99.9 atm). We assume a constant partial pressure of the $CO_{2(sc)}$ plume over time because $CO_{2(sc)}$ is delivered continuously by the plume for a long time and, for the sake of simplicity, we equate the partial pressure with the hydrostatic pressure.

3.3. Initial mineralogical composition of the reservoir and cap rock and initial brine compositions

Each cell is defined by specific mineralogical, hydrochemical and physical properties. A homogeneous distribution of relevant

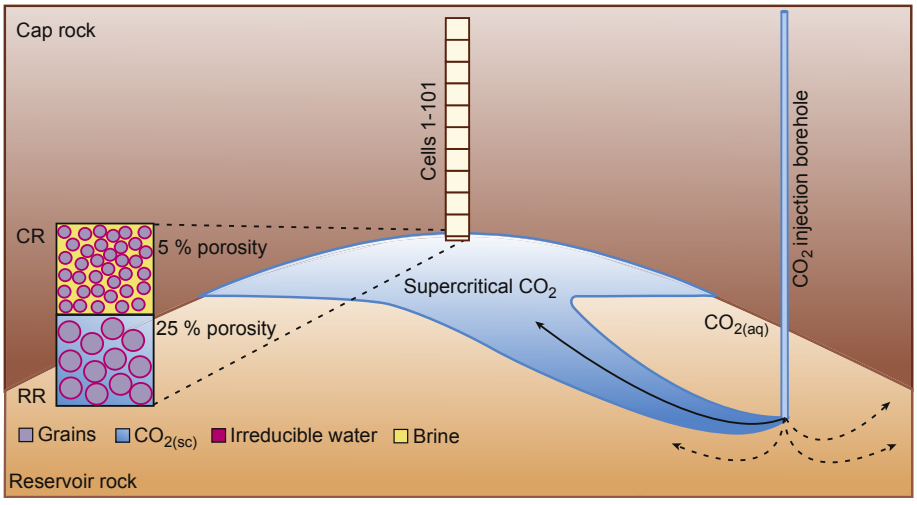

Fig. 1. System sketch of the model. CR = cap rock, RR = reservoir rock, $CO_{2(sc)}$ = supercritical CO_2 and $CO_{2(aq)}$ = aqueous CO_2.

parameters in the cap rock (cells 2–101) such as mineralogical composition is assumed. Table 1 summarizes the selected initial mineralogical composition in all cells. Assuming an initial total porosity of 25.0%, cell 1, representing the reservoir rock, is filled with 1.0 L of irreducible water, whereas 4.0 L of pore space are occupied by injected CO_2 ($CO_{2(sc)}$ plume).

Cells 2–101 are located in the cap rock and are characterized by a representative volume of 20.0 L with an initial porosity of 5.0% (1.0 L irreducible water and 19.0 L solid phases), where the type of porosity is neglected. The assumption of 5% initial porosity in the cap rock is based on observations from the Nordland Shale in UK Quadrant 16, northern North Sea [5,35] as an analog for the cap rock porosity in the CCS system Sleipner. Taking into account the specific density of each mineral phase (in g/cm^3), the amount of single mineral phases is calculated in mole per kg of pore water for different reservoir parts (Table 1). It is assumed that a small amount of CO_2 prevails in the cap rock and the reservoir rock during burial prior to $CO_{2(sc)}$ injection ($\rho CO_2 = 1.0$ atm). Before CO_2 injection and the triggered diffusion, a separate batch modeling calculates the initial composition of brines in both reservoir parts (the detailed input file for the separate batch model to calculate the cap rock brine is given in the Supplementary material). The brine composition of cell 1 (reservoir rock) is calculated by equilibrating 1 L of 1.5 M Na^+/Cl^--dominated solution with the defined primary minerals and gas phase under 40.0 °C and 100.0 atm (Table 2). For calculating the initial brine composition in cells 2–101 (cap rock), a 1.5 M Na^+/Cl^--dominated solution including 0.15 mol/kgw K^+ is equilibrated with the mineral phases of the cap rock and CO_2 under the pre-assigned reservoir P–T gradient (cell 2: 39.967 °C and 99.9 atm; cell 3: 39.934 °C and 99.8 atm; Table 2).

4. Methodology

The software PHREEQC Interactive 3.1.4–8929 [36] and its database phreeqc.dat are the modeling tools for the one-dimensional reactive transport modeling. This software is provided by the Geological Survey of the United States. PHREEQC is based on an ion-association aqueous model and has the capability to simulate speciation, batch-reaction, one-dimensional transport and inverse geochemical calculations. The calculations are based on mass action laws that include all species used in this study (Al, Ba, C, Ca, Cl, Fe, K, Mg, Na, S, Si) and their corresponding equilibrium constants. A basic of the modeling is the thermodynamic database which includes the elements used in the model with their species (aq, s, g), mass-action equations, and equilibrium constants. The activity coefficients of species are calculated by using the Debye-Hückel equation. The one-dimensional reactive transport model calculation in PHREEQC is based on the Advection-Reaction-Dispersion Equation (ARD):

$$\frac{\partial C}{\partial t} = -v\frac{\partial c}{\partial t} + D_L\frac{\partial^2 C}{\partial x^2} - \frac{\partial q}{\partial t}, \quad (3)$$

where C is the concentration in water (mol/kgw), t is the time (s), v is the pore water flow velocity (m/s), x is the distance (m), D_L is the hydrodynamic dispersion coefficient [m^2/s, $D_L = D_e + \alpha_L v$, with D_e the effective diffusion coefficient, α_L the dispersivity (m)], and q is the concentration in the solid phase (expressed as mol/kgw in the pores).

Our model considers a multiple web of hydrogeochemical reactions including 119 aqueous species, 10 mineral phases and their interplay. We use PHREEQC Version 3 which considers the pressure and the temperature dependence of the mass-action law constants for the equilibrium reactions of the aqueous, gaseous and solid species involved. Table 3 shows the equilibrium phases, mass-action equations and equilibrium constants used in the model. Phases like dawsonite and nahcolite that are not present in the phreeqc.dat database are taken from the llnl.dat database and added to the input files. However, the pressure dependence of both minerals is not considered for either.

Numerous publications confirm that PHREEQC produces correct results by comparing the results with other codes [37–39]. A detailed comparison of modeling results of different software packages like The Geochemist's Workbench, EQ3/6, FactStage/ChemApp and PHREEQC is given by Haase et al. [40] with the focus on geochemical modeling of CO_2 and calcite dissolution in NaCl solutions. Furthermore, the user's manual of PHREQC provides calculations to verify their results [36].

4.1. Discretization

To check the numerical accuracy of the results, the total time, number of shifts and number of cells are refined, and the model

Table 1
Mineralogical composition of the reservoir rock and the cap rock.

Primary minerals	Weight percent [wt%]	Amount [mol/kgw]
Reservoir rock		
K-feldspar	14.0	19.952
Albite	5.0	7.563
Quartz	75.0	495.130
Calcite	6.0	23.778
Cap rock		
K-feldspar	6.0	10.991
Albite	3.0	5.833
Quartz	55.0	466.745
Calcite	5.0	25.471
Kaolinite	25.0	49.377
Pyrite	2.0	8.499
Chlorite	2.0	1.835
Barite	2.0	4.369

Table 2
Initial irreducible water composition of the reservoir rock and cap rock.

Parameter	Reservoir rock	Cap rock
pH	6.064	7.912
Temperature [°C]	40.0	39.967
Elements	Concentration [mol/kgw]	Concentration [mol/kgw]
Al	3.544e−06	5.13e−07
Ba	–[d]	3.46e−04
C_{tot}[a]	4.254e−02	2.52e+00
Ca	1.365e−02	1.96e−05
Cl[b]	1.500e+00	1.61e+00
Fe	–[d]	2.91e−07
K	7.649e−03	2.36e−02
Mg	–[d]	5.75e−03
Na[b]	1.492e+00	4.47e+00
S_{tot}[c]	–[d]	3.46e−04
Si	1.105e−04	6.56e−05

[a] C: summed concentration of aqueous CH_4 and C(+IV) species.
[b] Due to high Na^+ and Cl^- concentrations and the resulting high ionic strength the Pitzer database and Pitzer equations should be used but the Pitzer database does not include Si- und Al^{3+}-containing aqueous species and silicate minerals, which are important components of the cap rocks of CO_2 storage systems. Therefore, the phreeqc.dat is used, which includes such species and silicate minerals and uses the Debye–Hückel equation, even if the activity coefficients for all aqueous species are overestimated [16]. Parkhurst and Appelo [24] assert that "in sodium chloride dominated systems, the model may be reliable at higher ionic strengths". Furthermore, the results of the different sensitivity scenarios are compared in relation to one another and not in an absolute context.
[c] S: summed concentration of aqueous S(+VI) and S(-II) species.
[d] Not present.

Table 3
Equilibrium phases, mass-action equations and equilibrium constants used in the model. Data from phreeqc.dat, but dawsonite and nahcolite are from llnl.dat [35].

Equilibrium phase	Equilibrium reaction	log K at 25 °C, 1 bar
K-feldspar	$KAlSi_3O_8 + 8H_2O = K^+ + Al(OH)_4^- + 3H_4SiO_4$	−20.573
Albite	$NaAlSi_3O_8 + 8H_2O = Na^+ + Al(OH)_4^- + 3H_4SiO_4$	−18.002
Quartz	$SiO_2 + 2H_2O = H_4SiO_4$	3.98
Calcite	$CaCO_3 = CO_3^{2-} + Ca^{2+}$	8.48
Kaolinite	$Al_2Si_2O_5(OH)_4 + 6H^+ = H_2O + 2H_4SiO_4 + 2Al^{3+}$	7.435
Pyrite	$FeS_2 + 2H^+ + 2e^- = Fe^{2+} + 2HS^-$	−18.479
Chlorite(14A)	$Mg_5Al_2Si_3O_{10}(OH)_8 + 16H^+ = 5Mg^{2+} + 2Al^{3+} + 3H_4SiO_4 + 6H_2O$	68.38
Barite	$BaSO_4 = Ba^{2+} + SO_4^{2-}$	−9.97
Dawsonite	$NaAlCO_3(OH)_2 + 3H^+ = Al^{3+} + HCO_3^- + Na^+ + 2H_2O$	4.35
Nahcolite	$NaHCO_3 = HCO_3^- + Na^+$	−0.11
$CO_{2(g)}$	$CO_2 = CO_2$	−1.468

calculation for one (the same) scenario is rerun and the results are compared [36,41]. Using a non-reactive tracer, induced as a peak injection into the first cell of the model, the progress of diffusion can be demonstrated. A concentration gradient for the non-reactive tracer is chosen based on CO_2 molality at the temperature and pressure conditions in the reservoir rock and in the cap rock. Thereby the diffusive mass transport progress of CO_2 can be tested, if the CO_2 would not react with the brine and the mineral phases of the cap rock. The total time, number of shifts and number of cells are refined until ions moved from regions of high concentration (cell 1) to regions of lower concentration (cells 2–101), resulting in an equal concentration in all cells (1–101).

To define the total time a non-reactive tracer is induced in the model to calculate the time at which the tracer concentration is equal in all cells. The model calculation is repeated for a total time of 10^4, 10^5, 10^6 and 10^7 years with a constant number of shifts and cells. The results show that the tracer concentration is equal in all the cells in the models at times of one million and ten million years (Table 4). In the following models the time scale of one million years is chosen.

In the second step of refinement the number of shifts is varied. The time is kept constant to one million years but the number of shifts (100, 1000, 10,000) and therefore the length of the time steps is varied, although PHREEQC may subdivide the "time step into smaller dispersion time steps if necessary to calculate dispersion accurately" [36]. Table 4 shows identical results for all the modeled numbers of shifts in the last shift. When comparing the tracer concentration at a fixed time for all models, differences in the progress of the diffusion are identifiable. The tracer concentration 1000 years later is equal in all cells in the 1000-shifts model to that in the model with 100 shifts. With 10,000 shifts the tracer concentration 400 years later is equal in all cells to that with 1000 shifts. The stopping criterion is set to 1‰, so 400 years fall below this cut-off. Therefore, the relevant number of shifts is set to 1000.

In the last step of refinement, the number of cells is varied (11, 21, 51, 101). The total time is kept constant to one million years and the number of shifts are kept constant to 1000. Table 4 depicts identical results for all the modeled numbers of cells in the last shift. The same procedure as for identification of the number of shifts applies here. When comparing the tracer concentration at a fixed time for all models, differences in the progress of the diffusion are identifiable. Considering the stopping criterion of 1‰, the results show that the relevant number of cells is 101 (Table 4).

Table 4
Results of temporal-spatial refinement rounded to two decimal places. The parameters used for the reference scenario are shown in bold. [a] = last cell: 101, [b] last cell: 11, [c] last cell: 21, [d] last cell: 51.

Parameters	Tracer concentration $C_{(tracer)}$ [mol/kgw]		
	Cell 1	Last cell	ΔC_{tracer}
$Time_{total}$ [a]			
0.00	0.85	0.01	0.84
10,000	0.06	0.01	0.05
100,000	0.03	0.01	0.02
1,000,000	0.02	0.02	10^{-6}
10,000,000	0.02	0.02	10^{-6}
Shifts			
100	0.02	0.02	10^{-6}
1000	0.02	0.02	10^{-6}
10,000	0.02	0.02	10^{-6}
Cells			
11[a]	0.10	0.09	0.01
21[b]	0.06	0.04	0.02
51[c]	0.06	0.01	0.05
101	1.04	0.99	0.05

These results are valid for the model of the reference scenario only and discretization studies should be done for each 1DRMT model. Numerical stability/instability is time and space dependent. To achieve numerical stability, the grid and time steps have to be refined, but due to the smaller time steps the number of solution calculations increases [36]. Moreover, the change in concentration, which results from reactions, is small from one time step to the next [42]. A disadvantage of this method is that it is not clear how many cells and which length of time step are necessary to achieve numerical stability [42].

Similar to our study, other studies like that of Mohd Amin et al. [16] consider numerical dispersion as well, but they assert that their "results are not sensitive to numerical dispersion and other errors in the discretization of the transport and reaction equations" [16]. They substantiate their assertion with a half of the grid spacing and the outcome of identical results. The results presented here show the opposite effect with a strong sensitivity to numerical dispersion in the sense of Mohd Amin et al. [16]. The reason for that difference is the assumption of a non-reactive tracer. CO_2 (used by Mohd Amin et al. [16]) reacts with the reservoir and cap rocks and the respective formation waters, so an equal tracer concentration in all cells is reached earlier than without a non-reactive tracer. The advantage of a non-reactive tracer is that the progress of diffusion over the total time and the total distance (=number of cells) can be demonstrated independently from the chemical reactions that may occur. Furthermore, Credoz et al. [6] assume a total time for the long-term safety assessment of CCS of 10,000 years. Based on the results of the discretization for this model, a total time of 1,000,000 years is defined. However, we are aware that the assumed physical and chemical conditions, as well as the use of a non-

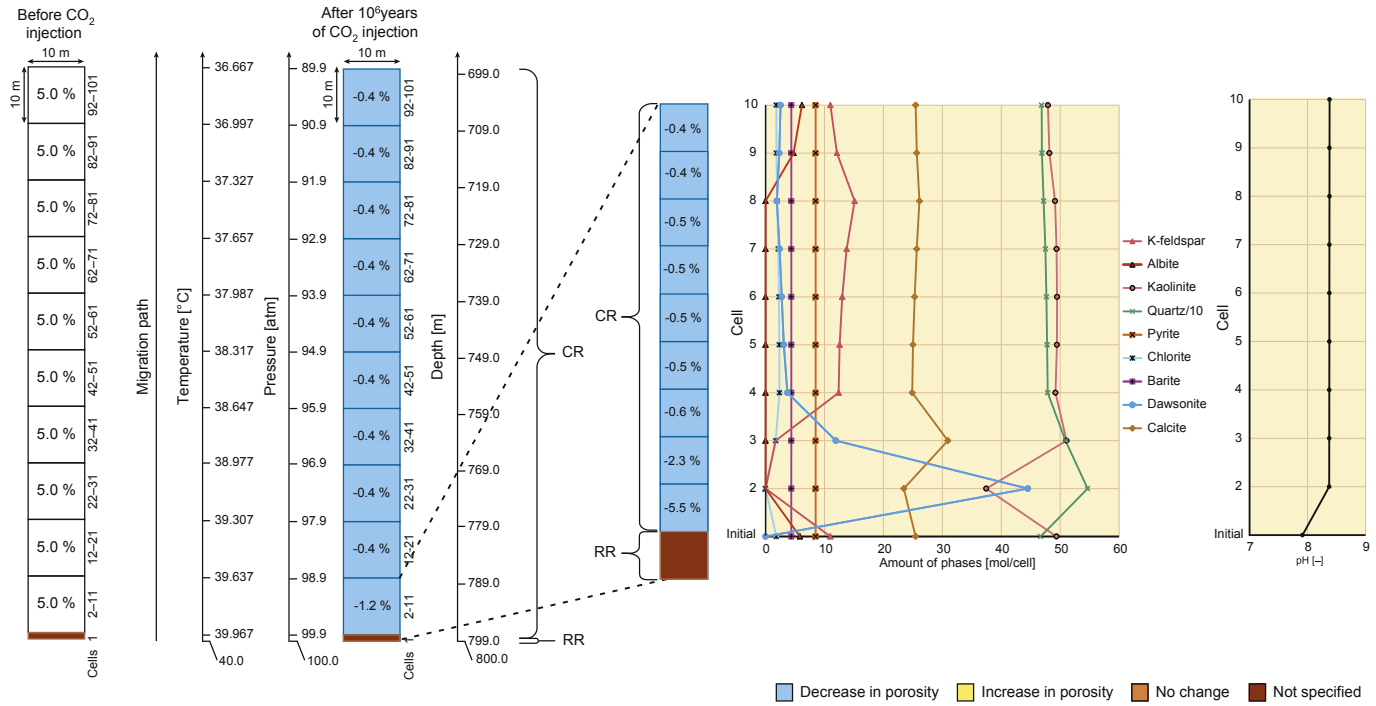

Fig. 2. Initial conditions in the column of 101 cells and calculated distribution of changes in porosity in %, mineral amounts as well as pH for the reference scenario after 10^6 years. RR = reservoir rock, CR = cap rock. "Initial" shows the initial mineralogical composition of the cap rock and the initial pH of the cap rock brine. Cell 2 is completely cemented. The porosity is reduced from the initial 5.0% to −0.5% after 10^6 years (= decrease in porosity of −5.5%). The amount of precipitated phases is higher than the available pore space. Consequently, the phases will use the available pore space in the next cell.

reactive tracer, do not comply with a real system and cannot represent the complexity of the system. Nevertheless, checking the numerical accuracy of the modeling results is essential for all modeling studies.

5. Results and discussion

5.1. Reference scenario

The equilibrium species distribution and the mass conversion are calculated based on the chemical thermodynamics of aqueous equilibrium reactions. The results of the 1DRMT model after 10^6 years of diffusive mass transport are shown in Fig. 2 where the column of 101 cells and the change of porosity for the reference scenario are depicted. Cell 1 is neglected because it is positioned in the reservoir rock and has a different initial mineralogical composition, whereas all the other cells are located in the cap rock. The modeling results show that the mineral dissolution and precipitation differ from cell to cell, whereat mass conversion occurs predominantly in cells 2–9. Therefore, the calculated results within the first ten cells are shown enlarged and are discussed in detail (Fig. 2.).

The cap rock brine dissolves the $CO_{2(sc)}$ and free H^+ are released because of carbonic acid dissociation. Due to acid attack, albite, K-feldspar and calcite dissolve and the corresponding pH increases to 8.4. Cell 2 is completely cemented after 10^6 years. The porosity is reduced from the initial 5.0% to −0.5% (Δ −5.5%). The negative value (−0.5%) implies that the amount of precipitated phases is higher than the available pore space. Consequently, the phases cement also the available pore space in the next cell. Mineral dissolution and precipitation reactions are expressed by the Saturation Index (SI) = log (IAP/K) (IAP: ion activity product; K: solubility product). When $CO_{2(aq)}$ migrates into cell 2 the cap rock brine is temporarily oversaturated with respect to quartz and dawsonite (SI > 0) and undersaturated regarding K-feldspar, albite, kaolinite, calcite, chlorite and barite (SI < 0). Thereupon, quartz and dawsonite precipitate in high amounts (+124.3 mol in cell 2) and K-feldspar, albite, kaolinite, calcite, chlorite and barite dissolve in small amounts (−32.6 mol in cell 2). The dissolution of albite and K-feldspar contributes Na^+, K^+, $Al(OH)_4^-$ and H_4SiO_4 to the cap rock brine. To form dawsonite, Al^{3+} and Na^+ have to react with HCO_3^- and $2H_2O$ and reach saturation with $SI_{dawsonite} > 0$. The respective equilibrium reactions are given in Table 3. Fig. 2 shows that with increasing dissolution of albite and K-feldspar the precipitation of dawsonite gets stronger. Calcite dissolves in cell 2 in small amounts only. Calcite dissolves slightly more strongly when albite and K-feldspar are completely dissolved, but the amount of both in this model is high enough to buffer the pH and protect calcite against stronger dissolution.

In cell 3 the porosity decreases from the initial 5.0% to 2.7% (Δ −2.3%). The precipitation of quartz, dawsonite, calcite and kaolinite is responsible for this decrease. The dissolution of K-feldspar, albite and chlorite in comparison with the precipitation of quartz, dawsonite, calcite and kaolinite is too weak to create an increase in porosity. In cell 4 a weaker decrease in porosity from the initial 5.0% to 4.44% is observable. Quartz, dawsonite, K-feldspar, chlorite all precipitate and albite, kaolinite and calcite dissolve.

From cell 5 to cell 9 the porosity decreases from the initial 5.0% to ~4.5%. Quartz, dawsonite, K-feldspar and chlorite precipitate in these cells, whereas albite dissolves. Calcite dissolves in cells 5 and 6 but precipitates in small amounts in cells 7–9. Kaolinite precipitates in cells 5–7 and dissolves in cells 8 and 9. Cells 10 to 101 show similar results. Dawsonite precipitates as well as quartz, albite, K-feldspar, chlorite and barite. Kaolinite and calcite dissolve. Albite is completely dissolved from cells 2–8 but precipitates in small amounts from cell 9 onwards. Simultaneously, dawsonite precipitation decreases and kaolinite dissolution starts. Precipitation and dissolution of pyrite, barite and chlorite has a low intensity and can be neglected.

Hellevang et al. [43] discussed the potential of dawsonite to permanently trap CO_2 and assumed that "if dawsonite does precipitate at nonalkaline conditions it is only an ephemeral phase which decomposes when CO_2 pressure drops". Using nahcolite ($NaHCO_3$) as potential secondary phase instead of dawsonite ($NaAlCO_3(OH)_2$), the decrease in porosity is with a mean of −1.0% in cells 2–10 and of −0.3% in cells 11–101 smaller than using dawsonite (−1.2% in cells 2–10 and −0.4% in cells 11–101). The difference in the results can be explained by a smaller amount of precipitated nahcolite in comparison with dawsonite. By dissolution of albite and K-feldspar, Na^+ and Al^{3+} ions are available. Nahcolite can use Na^+ ions only, whereas dawsonite uses Na^+ and Al^{3+} ions. It is striking that calcite and kaolinite precipitate when previously formed secondary nahcolite is available. The pH is 8.1 when using nahcolite as the potential secondary phase, whereas dawsonite precipitation leads to a pH of ca. 8.4.

Table 5
Parameter sensitivity analysis in alternative scenarios.

Scenario	Parameter	
Reference	Temperature/pressure	40.0–36.7 °C/100.0–90.0 atm
1a		150.0–146.7 °C/470.0–460.0 atm
1b		60.0–56.7 °C/150.0–140.0 atm
1c		34.0–30.7 °C/60.0–50.0 atm
Reference	Veins	No veins
2a		Quartz vein (100% quartz, 5.0% porosity)
2b		Calcite vein (100% calcite, 5.0% porosity)
2c		Calcite vein (100% calcite, 5.5% porosity)
2d		Calcite vein (100% calcite, 40.0% porosity)
Reference	Initial cap rock porosity	5.0%
3a		40.0%
3b		10.0%
3c		6.0%
3d		2.0%
Reference	Effective diffusion	3.33×10^{-10} m^2/s
4a	coefficient	1.00×10^{-10} m^2/s
4b		4.50×10^{-11} m^2/s
4c		1.00×10^{-11} m^2/s
Reference	Injected fluid	100% CO_2
5a	composition	99.0% CO_2 + 1.0% CH_4
5b		50.0% CO_2 + 50.0% CH_4
5c		99.0% CO_2 + 1.0% H_2S
Reference	Initial conditions	–
6a	according to published case study	Mineralogical data from Bildstein et al. [10] (see Appendix Table A 1, Table A 2)
6b		Mineralogical data + P–T conditions from Bildstein et al. [10] (see Appendix Table A 1, Table A 2)
Reference	Transport mechanism	Diffusion
7		Advection
Reference	Temperature	40.0–36.7 °C/100.0–90.0 atm
8a		150.0–146.7 °C + constant pressure (469.9 atm)
8b		34.0–30.7 °C + constant pressure (59.9 atm)
Reference	Pressure	40.0–36.7 °C/100.0–90.0 atm
9a		470.0–460.0 atm + constant temperature (149.967 °C)
9b		60.0–50.0 atm + constant temperature (33.967 °C)

5.2. Alternative scenarios

Table 5 shows the input parameters used in the alternative scenarios. All the alternative scenarios are based on the reference scenario, and single parameters are changed to show their effects on the modeling results of each parameter. The modeling results of the alternative scenarios are presented in Fig. 4.

5.2.1. Temperature/pressure

Scenarios 1a–c cover a spectrum of temperature and pressure conditions, comparable to CO_2 storage systems like those at Ketzin (Germany), Frio (USA) and Lacq-Rousse (France). Changing temperature and pressure will affect the equilibrium constants, K^a, of the mass-action laws of minerals, aqueous species and gases in such CO_2 dominated systems [18]. Thus, scenarios 1a–c show the effect of temperature and pressure on the change in porosity triggered by mineral dissolution and precipitation. The pH varies for the different scenarios. It decreases in scenario 1a to 6.7 but increases in scenario 1b to 8.0 and in scenario 1c to 8.5–8.6. At a temperature of 150.0 °C and a pressure of 470.0 atm the porosity of the cap rock increases from the initial 5.0% to up to 6.7% in cells 12–101. At a temperature of 60.0 °C and a pressure of 150.0 atm the porosity of the cap rock decreases from the initial 5.0% to up to 4.8% in cells 12–101. At P–T conditions of 60.0 atm and 34.0 °C the porosity decreases from the initial 5.0% to 4.5% in cells 12–101. At temperatures between 34.0 °C and 135.0 °C and pressures between 60.0 atm and 440.0 atm the porosity decreases from the initial 5.0% to an average of 4.4%. With the help of various further temperature/pressure scenarios, a critical point is revealed where the porosity development changes from a decrease to an increase. This critical point lies between the temperatures of 135.0 °C and 150.0 °C and corresponding pressures of 440.0 atm and 470.0 atm.

Changes in temperature and pressure affect the mineral behavior. When comparing scenario 1a (150.0 °C/470.0 atm; cell 1) with the reference scenario (40.0 °C/100.0 atm; cell 1), differences in the porosity change are identifiable. At higher temperature and pressure conditions (scenario 1a) the porosity increases. Unlike the reference scenario where the pH increases from the initial 7.9 to 8.4, the pH decreases to 6.7 in scenario 1a. In contrast to the reference scenario, in scenario 1a chlorite is completely dissolved in cells 2–101. K-feldspar is completely consumed in the first cells but is available from cell 5, one cell earlier than in the reference scenario. Calcite, quartz and kaolinite dissolution and precipitation are less strong than in the reference scenario. The same applies for dawsonite, which precipitates with 44.5 mol in cell 2 in the reference scenario and with 23.3 mol in cell 2 of scenario 1a.

5.2.2. Veins

Cap rock properties like mineralogical compositions rarely show a homogeneous distribution. Quartz veins and calcite veins occur frequently. For this, scenarios 2a–d with monomineralogical compositions of quartz and calcite are calculated (Fig. 4, Table 5). In a quartz vein, a small decrease in porosity is observed in cell 2 (−0.01% from the initial 5.0%), while the porosity change in all other cells is <0.01%. The same results apply for scenario 2b considering a calcite vein and an initial porosity of 5.0%. Calcite veins with a higher initial porosity of 5.5% (scenario 2c) lead to a decrease in porosity in cell 2 (−0.01%) and to a weak increase in all other cells (Δ + 0.01%). This trend is measurable up to an initial porosity of 10.0%. Another scenario (2d) considers an initial porosity of 40.0% in the calcite veins, as modeled by Bildstein et al. [10]. Despite such a high initial porosity of 40% in calcite veins, the modeling results show a decrease in porosity of −0.05% in cell 2 but constant porosities in the following cells. In summary, secondary porosity can be created when the initial porosity ranges between ~5.2% and ~10%. The pH in the cap rock brine decreases from 7.9 to 6.8 in all four scenarios (2a–d) and is lower than in the reference scenario (pH 8.4).

5.2.3. Initial cap rock porosity

With a scenario series (3a–d) different initial cap rock porosities between 2.0% and 40.0% are calculated to test the effects of this parameter. The high initial cap rock porosity of 40% conceptually represents that open fractures occur in the cap rock. The modeling results with an initial cap rock porosity of 40.0% show a strong decrease in porosity in cell 2 (−16.34%), a decrease of between 8.34% and 31.66% (ø −9.5%) in cells 3–12 and a −3.4 to −3.7% loss in porosity for cells 13–101. This trend is also traceable for initial porosities of 10.0%, 6.0% and 2.0%, as well as for the reference scenario with an initial porosity of 5%. The pH of the cap rock brine lies between 8.4 and 8.5 in all scenarios (3a–d).

5.2.4. Effective diffusion coefficient

Scenarios 4a–c aim to unravel the effects of diffusion intensity by varying the effective diffusion coefficients from 1.00×10^{-10} m^2/s [10], 4.50×10^{-11} m^2/s [5] to 1.00×10^{-11} m^2/s [10]. As in the reference scenario, the pH in the cap rock brine increases in all scenarios (4a–c) to ~8.4. Despite a broad range of diffusion coefficients, similar results indicate that the diffusion intensity has no effect on changes in porosity (Fig. 4). However, this conclusion is only valid for the assumed chemical, physical and mineralogical conditions.

5.2.5. Injected fluid composition

Based on the study by Mohd Amin et al. [16], several scenarios consider various compositions of injected fluids, including CH_4 and H_2S mixtures with the main component CO_2. Assuming an ideal gas behavior in the gas mixtures, the fugacity coefficients will be calculated for the gas components. Modeling results of scenario 5a (99.0% CO_2 + 1.0% CH_4) show a strong decrease in porosity in cells 2 and 3 (from the initial 5.0% to 0.0%–3.07%) and a moderate decrease in porosity in the remaining cells (down to ~4.57%). An increase in the concentration of CH_4 in the injected fluids from 1.0% to 50.0% leads to a weaker decrease in the porosity in cells 2 and 3 but similar values in the remaining cells. The addition of 1.0% H_2S in scenario 5c decreases the porosity in cell 2, down to 2.79% in cell 3, whereas the porosity increases slowly up to 4.57% in cell 10 and stays constant in the remaining cells. Summarizing, the main differences in porosity change, when using the various fluid compositions, are identifiable in the first cells (2–10) where the change varies from −0.6% to −1.2%. The porosity changes in cells 11–101 are independent of the injected fluid composition (from pure CO_2 to CH_4 and H_2S mixtures; Figs. 2 and 4.). Similar to the reference scenario, the pH increases in scenarios 5a–c to ~8.4. As mentioned by Mohd Amin et al. [16], when using CH_4 and H_2S mixtures with the main component CO_2, the porosity in the cap rock decreases and the sealing capacity of the cap rock increases.

5.2.6. Initial conditions according to published case study

In comparison with our reference scenario, Bildstein et al. [10] used a different mineral assemblage in the cap rock, including illite, anhydrite, kaolinite, quartz, pyrite, ankerite, Ca-montmorillonite and calcite (for percentages see Appendix). Scenario 6a considers the same mineral assemblage under the pressure and temperature conditions of the reference scenario. In scenario 6a the cap rock porosity decreases in cell 2 (Δ −0.7%), to 2.0% in cell 3 and to 4.3% in cell 4 (Fig. 3.). In the following cells,

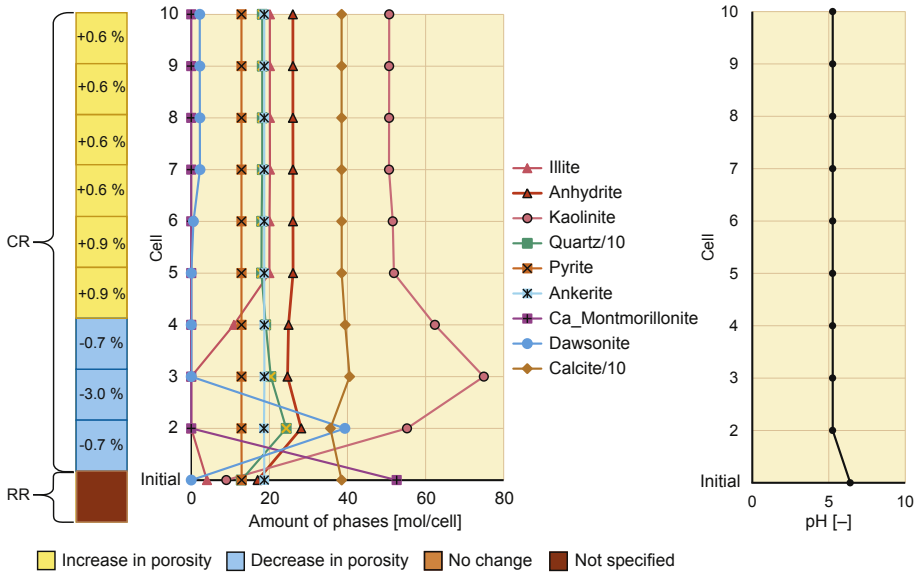

Fig. 3. Gain or loss of total porosity and mass conversion of the minerals for scenario 6a in the first 10 cells with a cell length of 1 m. 9 m are located in the cap rock (CR) and 1 m in the reservoir rock (RR).

the porosity increases to 5.9% (cells 5 and 6) and remains constant at ~5.6% (cells 5–101). In cells 5–101 illite, quartz, ankerite, and dawsonite precipitate and anhydrite, kaolinite, calcite, and Ca-montmorillonite dissolve. Another scenario (6b) uses the P–T conditions and the mineral assemblage given by Bildstein et al. [10]. In this scenario, the porosity of the cap rock decreases to 1.11% in cell 2 but shows a strong increase in cell 2 to 7.46%. The average for the cells 11–101 lies at 6.2% (Fig. 4). In scenario 6a the pH in the cap rock brine decreases from 6.54 to ~5.3 and in scenario 6b the pH increases to 10.4.

5.2.7. Advection as transport mechanism

The ability of the cap rock to safely store CO_2 depends, amongst other factors, on the reservoir pressure. If the reservoir pressure becomes too large, new fractures and faults are created [44] and pose a high risk of CO_2 leakage. Scenario 7 simulates an intensive CO_2 leakage in fractures and faults by considering advection as the transport mechanism instead of diffusion in the reference scenario. Compared to diffusion, advection enables a faster, stronger and more expansive spread of CO_2. This leads to a lower pH in scenario 7 (to 3.3–5.0 in cells 2–13 and 6.9–7.1 in cells 14–101) compared to 8.4 in all cells of the reference scenario. Such a strong decrease in pH accompanies the complete dissolution of K-feldspar, albite, kaolinite, calcite, chlorite in cells 2–13. However, no secondary porosity is created in these cells because the volume of newly formed quartz and dawsonite overcompensates the volume resulting from dissolution of K-feldspar, albite, kaolinite, calcite, chlorite.

5.2.8. Changing temperature at a constant pressure

Scenarios 1a–c reveal the change in porosity in dependence on temperature and pressure. In contrast, in scenarios 8a + b only the temperature is changed and the pressure is set constant to show the effect of temperature on the porosity change. However, a constant pressure assumed in these scenarios does not comply with a real system. In scenario 8a, change in porosity is limited to cells 2 to 11: increases by 0.7% in cell 2 and decreases by −1.1% on average in cells 3–11. Such calculated changes in porosity are less intensive when compared to scenario 1a. When comparing these results with the results of scenario 1a strong differences are observed in cell 2. In scenario 1a the porosity decreases and in scenario 8a the porosity increases. In cell 3 to 11 the opposite effect is detectable. Whereas the porosity increases in scenario 1a, it decreases in scenario 8a. The pH of the cap rock brine for both scenarios (8a and 1a) decreases from the initial 7.9 to 6.7. In scenario 8b the calculated porosity decreases in all cells, which is similar to scenario 1c. The difference with scenario 1c (in which the temperature and pressure are changed) is detectable in cell 2 only where a difference in the third decimal place is observed. Even the pH of the cap rock brine (8.5–8.6) is the same in scenario 8b and 1c. In summary, scenarios 8a and 8b show that the temperature has a stronger effect on mineral dissolution and precipitation at high pressure and temperature conditions.

5.2.9. Changing pressure at constant temperature

Scenarios 9a + b aim to test the influence of pressure on mineral dissolution and precipitation. In scenario 9a, the porosity increases in cell 2 but decreases in cell 3–11, whereas no change in the remaining cells is observable. In contrast, in scenario 1a the porosity decreases in cell 2 only, while all other cells show a porosity increase. As in scenario 1a, the pH of the cap rock brine decreases from the initial 7.9 to 6.7 in scenario 9a.

The modeling results of scenario 9b show that the porosity decreases in all cells. When comparing the results between scenario 9b and scenario 1c (where the temperature and pressure are changed), differences are detectable in the third decimal place in cells 2 and 3 only. The same applies for the pH of the cap rock brine, which increases to 8.5 in scenario 9b and to 8.5–8.6 in scenario 1c. Like the effect of temperature (scenarios 8a + b), the effect of pressure on the change in total porosity is stronger at higher temperature and pressure conditions. Comparing the effect of temperature with the effect of pressure on porosity change, only small differences are identifiable. The pressure effect is slightly stronger than the temperature effect but there are differences in the second decimal place.

5.3. Sensitivity analysis

The sensitivity analysis aims to show the effect of different solubility constants for $CO_{2(g)}$ on the modeling results. We vary

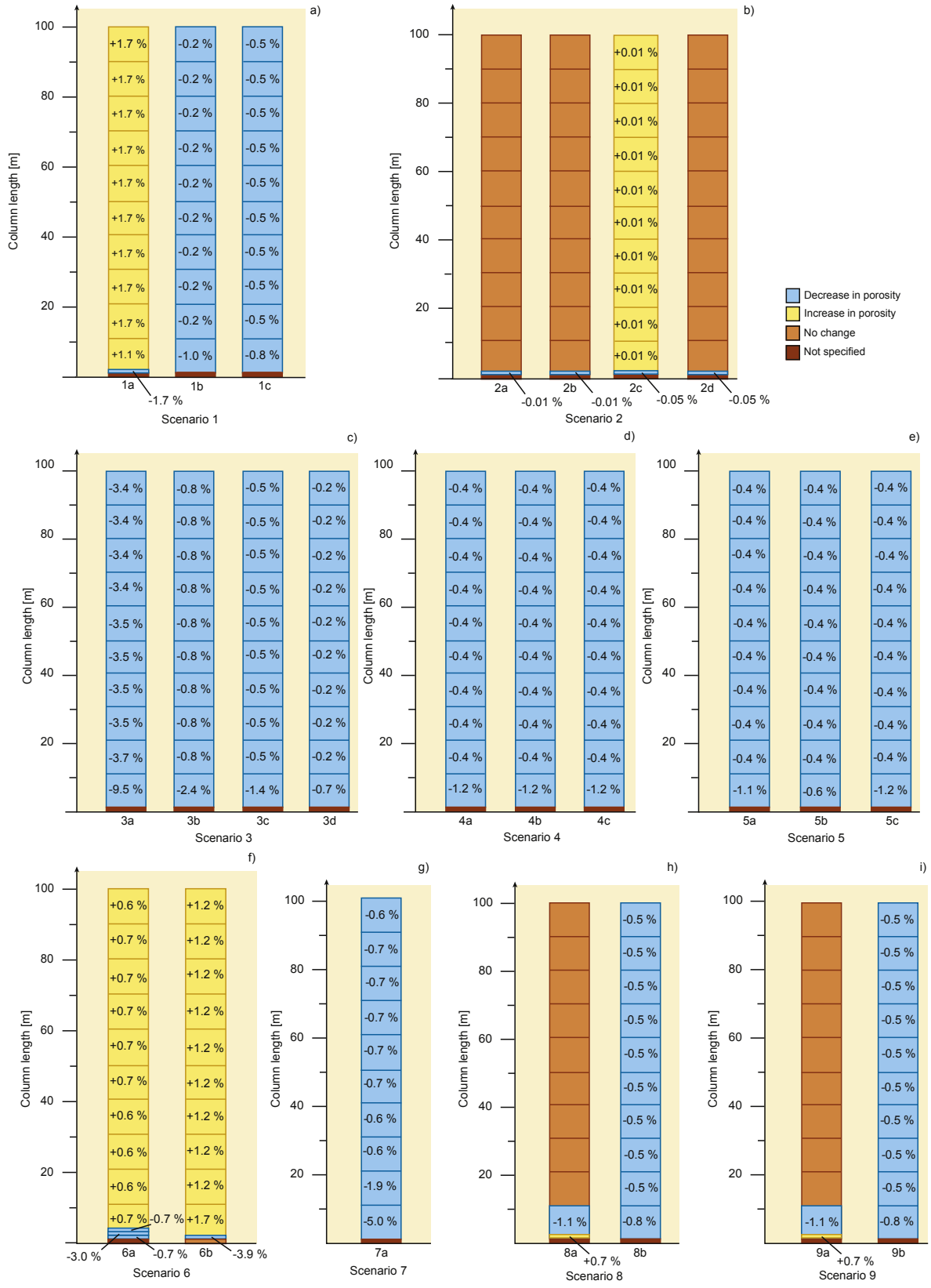

Fig. 4. Gain or loss of total porosity for scenarios 1 to 9 (a–i) in a column of 101 cells, with a cell length of 1 m. 100 m are located in the cap rock and 1 m in the reservoir rock. The values are given as mean values for every 10 m.

the log K values for $CO_{2(g)}$ from initial −1.468 to −1.769 and −1.167 for the reference scenario. These values are chosen by doubling the solubility constant and by reducing the solubility constant by 50%. The modeling results show that the solubility constant of $CO_{2(g)}$ influences the final simulation results. The strongest change in porosity is identifiable in cells 2–4 whereby

Table 6
Comparison of solubility constants of $CO_{2(g)}$ based on the change in total porosity in the reference scenario for cells 2–10. log K −1.468 is the solubility constant used in the reference scenario.

Solubility constant $CO_{2(g)}$	log K −1.769	log K −1.468	log K −1.167
Cells	Decrease in porosity [%]		
2	−7.2	−5.5	−4.4
3	−1.1	−2.3	−2.0
4	−0.4	−0.6	−1.6
5	−0.5	−0.5	−0.5
6	−0.5	−0.5	−0.5
7	−0.5	−0.5	−0.5
8	−0.5	−0.5	−0.5
9	−0.4	−0.4	−0.4
10	−0.4	−0.4	−0.4

the change in the following cells (5–10) is at most in the second decimal place (Table 6). However, the general trend of decreasing porosity in the reference scenario does not depend on the chosen solubility constant.

5.4. Modeling limitations

The model presented here uses thermodynamic equilibrium reactions and the local equilibrium assumption for CO_2 storage systems. It does not aim to reflect the complexity of the whole system. However, there is a general agreement that models enable critical analysis of a system and that "model testing and the evaluation of predictive errors lead to improved models and better understanding of the problem" [45].

Our modeling approach is based on assumptions regarding chemical and physical parameters. It excludes kinetic aspects of mineral dissolution/precipitation. The used database phreeqc.dat includes the pressure and temperature dependence of the mass-action law constants for the equilibrium reactions of many aqueous, gaseous and solid species involved but with the exception of the pressure dependence of dawsonite and nahcolite which may be of great relevance for simulating CO_2 storage systems.

For the sake of simplicity, it is neglected that the modeling results of one cell could change the initial parameters for the neighboring cells. Changes in porosity and permeability affect the tortuosity. Such changes should be adapted in every single cell after every time step of the modeling. There is no valid relationship between permeability and porosity because the permeability-porosity correlation is site-specific and depends on many geometric factors [46]. However, it is shown in laboratory experiments [47] as well as in field data [48] that even small reductions in porosity, resulting from mineral precipitation, can significantly reduce permeability. Furthermore, newly formed solid phases close pore throats and leads to stronger reductions in permeability [46].

Even if the diffusion coefficient is specific to each aqueous species, depending on the species type, pressure, temperature and interaction with other species [5], the used computer code PHREEQC only allows a uniform diffusion coefficient for all aqueous species of 3.33×10^{-10} m^2/s. Nevertheless, the modeling results indicate that a change in the diffusion coefficient has no effect on the calculated results. Regarding the diffusion of dissolved CO_2 in cap rock, Fleury et al. [49] suggest that the diffusion coefficients depend primarily on the porosity. Consequently, in real CO_2 storage systems the effective diffusion coefficient must be calculated not only in dependence on the species and temperature of each cell but also on the newly formed porosity, changed by CO_2–water–rock interactions, in each cell. Furthermore, a homogeneous distribution of relevant cap rock parameters is considered in our study. In contrast, a heterogeneous distribution of relevant cap rock parameters can lead locally to different results. Moreover, tests of different boundary conditions (constant, closed and flux) show no effects on the modeling results.

6. Conclusions

The application of the 1DRMT modeling presented in this study provides a good example of how such a modeling approach could (1) identify mineral dissolution and precipitation in the cap rock triggered by molecular diffusion of CO_2 and (2) quantify the resulting porosity change, even allowing for several limitations.

Because of hydrogeochemical reactions, the results of the reference scenario show a change in porosity from cell to cell over the length of 101 m after 10^6 years of diffusive mass transport. Quartz and dawsonite precipitate, whereas K-feldspar, albite, kaolinite, calcite, chlorite and barite dissolve. Compared to these dissolved minerals, the more intensive precipitation of quartz and dawsonite causes a decreasing cap rock porosity in the reference scenario. Generally, the main changes in porosity are identifiable close to the cap rock/reservoir rock contact.

Alternative scenarios for selected physical and chemical parameters were performed in this study to identify the key factors controlling the change in porosity. The modeling results show that the creation of porosity depends on different factors. The following conclusions are based on the results of the alternative scenarios.

(1) Mineral dissolution and precipitation and resulting porosity changes are temperature and pressure dependent, because temperature and pressure affect the mass-action laws of minerals and aqueous species involved in the equilibrium reactions. In the tested range of 30.7–150.0 °C and 50.0–470.0 atm, both temperature and pressure have a stronger effect on mineral dissolution and precipitation at higher P–T conditions. Therefore, it is important to consider that the initial temperature and pressure conditions can differ from location to location in a single system (i.e. in folded structures). Compared to temperature, the effect of pressure on the change of porosity is slightly stronger.
(2) Regarding temperature and pressure conditions, there is a critical point where the porosity development changes from decrease to increase. For the reference scenario the critical point lies between 135.0 °C and 150.0 °C and 440.0 atm and 470.0 atm. This critical point would vary when the initial conditions change, specifically the initial mineralogical compositions of the cap and reservoir rocks.
(3) Depending on the initial porosities, calcite, which frequently occurs as veins in cap rocks, can dissolve. Therefore, calcite veins could be a risk for the sealing capacity of the cap rock.
(4) When using initial cap rock porosities between 2.0% and 10.0%, a decrease in total porosity over the length of one hundred meters of modeled cap rock is identifiable. These results indicate that under the assumed physical, chemical and mineralogical conditions, the sealing capacity of the cap rock is improved.
(5) Using the mineralogical phase assemblage from Bildstein et al. [10], an increase in porosity from the fifth meter onwards is identifiable, so the sealing capacity of the cap rock decreases. This result indicates that porosity creation depends strongly on the mineralogical composition of the

reservoir and cap rock as well as on the brine compositions.

Appendix

Table A 1
Initial mineralogical data from Bildstein et al. [10] for parameter sensitivity analysis.

Temperature = 80 °C, ρCO_2 = 150 bar							
Initial mineralogical composition of the cap rock		Reservoir water		Acidified reservoir water		Initial cap rock water	
	Weight percent [wt%]	pH	6.24	pH	4.75	pH	6.54
Calcite	50	Species	Molality	Species	Molality	Species	Molality
Ankerite	5	Al	5.622×10^{-8}	Al	1.251×10^{-7}	Al	1.531×10^{-7}
Montmorillonite	25	C	4.895×10^{-3}	C	1.141	C	2.180×10^{-3}
Kaolinite	3	Ca	1.612×10^{-2}	Ca	3.204×10^{-2}	Ca	1.528×10^{-2}
Illite	2	Cl	3.014×10^{-1}	Cl	3.015×10^{-1}	Cl	2.601×10^{-1}
Quartz	10	Fe	2.137×10^{-7}	Fe	1.751×10^{-6}	Fe	1.534×10^{-5}
Anhydrite	3	K	2.374×10^{-3}	K	2.375×10^{-3}	K	1.190×10^{-2}
Pyrite	2	Mg	1.282×10^{-2}	Mg	2.424×10^{-2}	Mg	8.937×10^{-4}
		Na	2.594×10^{-1}	Na	2.595×10^{-1}	Na	2.543×10^{-1}
		S	7.642×10^{-3}	S	7.649×10^{-3}	S	1.841×10^{-2}
		Si	8.994×10^{-4}	Si	8.833×10^{-4}	Si	5.371×10^{-4}

Table A 2
Additional equilibrium phases, mass-action equations and equilibrium constants used in scenarios 6a–b. Data from phreeqc.dat [35], but ankerite is from Bildstein et al. [10].

Equilibrium phase	Equilibrium reaction	log K at 25 °C, 1 bar
Ankerite	$CaFe_{0.7}Mg_{0.3}(CO_3)_2 + 4H^+ + 0.7Fe^{2+} + 0.3Mg^{2+} + 2H_2O + 2CO_2$	12.14[a]
Montmorillonite	$Ca_{0.165}Al_{2.33}Si_{3.67}O_{10}(OH)_2 + 12H_2O = 0.165Ca^{2+} + 2.33Al(OH)^{4-} + 3.67H_4SiO_4 + 2H^+$	−45.027
Illite	$K_{0.6}Mg_{0.25}Al_{2.3}Si_{3.5}O_{10}(OH)_2 + 11.2H_2O = 0.6K+ + 0.25Mg^{2+} + 2.3Al(OH)^{4-} + 3.5H_4SiO_4 + 1.2H^+$	−40.267
Anhydrite	$CaSO_4 = Ca^{2+} + SO4^{2-}$	−4.39

[a] Log K at 80 °C and 1 bar.

(6) Even over a broad range tested, the intensity of diffusive mass transport has negligible effects on mineral precipitation and dissolution as well as on resulting changes in porosity.
(7) The injected fluid compositions affect the sealing capacity of cap rocks which can increase by mixing CO_2 with CH_4 and H_2S in comparison with pure CO_2 injection.
(8) An intensive CO_2 leakage in fractures and faults enables a faster and broader spread of CO_2, and consequently, could cause an earlier and stronger sealing risk.
(9) Compared to nahcolite, dawsonite precipitates in higher amounts and is one reason for the decrease in porosity. However, the potential of dawsonite to trap CO_2 permanently is still a point of discussion [43].

Therefore, the chemical and physical data of the cap and reservoir rocks and brine must be measured under in situ conditions to develop a numerical model for evaluating a specific CO_2 storage system. Various cap rock mineral phase assemblages should be exposed to different aqueous solutions, partial pressures of carbon dioxide and P–T conditions in long-term laboratory batch experiments to observe mineral dissolution and/or precipitation. These results should be reproduced by batch modeling using identical initial parameters. Such a combination of laboratory experiments and modeling should be performed to test the plausibility of the applied hydrogeochemical equilibrium model.

Acknowledgements

We would like to thank the anonymous reviewers for their constructive reviews that considerably improved the manuscript.

Appendix A. Supplementary data

Supplementary data related to this article can be found at http://dx.doi.org/10.1016/j.petlm.2016.11.010.

References

[1] S. Holloway, An overview of the underground disposal of carbon dioxide, Energy Convers. Manag. 38 (1997) 193–198.
[2] IPCC, Special Report on Carbon Dioxide Capture and Storage. Prepared by Working Group III of the International Panel of Climate Change, Cambridge University Press, Cambridge, United Kingdom/New York, NY, USA, 2005.
[3] I. Gaus, P. Audigane, L. André, J. Lions, N. Jacquemet, P. Durst, I. Czernichowski-Lauriol, M. Azaroual, Geochemical and solute transport modelling for CO_2 storage, what to expect from it? Int. J. Greenh. Gas Control 2 (4) (2008) 605–625.
[4] J.R. Black, S.A. Carroll, R.R. Haese, Rates of mineral dissolution under CO_2 storage conditions, Chem. Geol. 399 (2015) 134–144.
[5] I. Gaus, M. Azaroual, I. Czernichowski-Lauriol, Reactive transport modelling of the impact of CO_2 injection on the clayey cap rock at Sleipner (North Sea), Chem. Geol. 217 (3–4) (2005) 319–337.
[6] A. Credoz, O. Bildstein, M. Jullien, J. Raynal, J.-C. Pétronin, M. Lillo, C. Pozo, G. Geniaut, Experimental and modeling study of geochemical reactivity between clayey caprocks and CO_2 in geological storage conditions, Energy Procedia 1 (1) (2009) 3445–3452.
[7] M. Fleury, J. Pironon, Y.M. Le Nindre, O. Bildstein, P. Berne, V. Lagneau, D. Broseta, T. Pichery, S. Fillacier, M. Lescanne, O. Vidal, Evaluating sealing efficiency of caprocks for CO_2 storage: an overview of the Geocarbone Integrity Program and results, Energy Procedia 4 (2011) 5227–5234.
[8] F. Gherardi, T. Xu, K. Pruess, Numerical modeling of self-limiting and self-enhancing caprock alteration induced by CO_2 storage in a depleted gas reservoir, Chem. Geol. 244 (1–2) (2007) 103–129.
[9] H. Tian, F. Pan, T. Xu, B.J. McPherson, G. Yue, P. Mandalaparty, Impacts of hydrological heterogeneities on caprock mineral alteration and containment of CO_2 in geological storage sites, Int. J. Greenh. Gas Control 24 (2014) 30–42.

[10] O. Bildstein, C. Kervévan, V. Lagneau, P. Delaplace, A. Crédoz, P. Audigane, E. Perfetti, N. Jacquemet, M. Jullien, Integrative modeling of caprock integrity in the context of CO_2 storage: evolution of transport and geochemical properties and impact on performance and safety assessment, Oil Gas. Sci. Technol. – Rev. IFP 65 (3) (2010) 485–502.
[11] B.L. Alemu, P. Aagaard, I.A. Munz, E. Skurtveit, Caprock interaction with CO_2: a laboratory study of reactivity of shale with supercritical CO_2 and brine, Appl. Geochem. 26 (12) (2011) 1975–1989.
[12] J. Wollenweber, S. Alles, A. Busch, B.M. Krooss, H. Stanjek, R. Littke, Experimental investigation of the CO_2 sealing efficiency of caprocks, Int. J. Greenh. Gas Control 4 (2) (2010) 231–241.
[13] Z. Szabó, H. Hellevang, C. Király, E. Sendula, P. Kónya, G. Falus, S. Török, C. Szabó, Experimental-modelling geochemical study of potential CCS caprocks in brine and CO_2-saturated brine, Int. J. Greenh. Gas Control 44 (2016) 262–275.
[14] P. Bolourinejad, R. Herber, Chemical effects of sulfur dioxide co-injection with carbon dioxide on the reservoir and caprock mineralogy and permeability in depleted gas fields, Appl. Geochem. 59 (2015) 11–22.
[15] H. Tian, T. Xu, Y. Li, Z. Yang, F. Wang, Evolution of sealing efficiency for CO_2 geological storage due to mineral alteration within a hydrogeologically heterogeneous caprock, Appl. Geochem. 63 (2015) 380–397.
[16] S. Mohd Amin, D.J. Weiss, M.J. Blunt, Reactive transport modelling of geologic CO_2 sequestration in saline aquifers: the influence of pure CO_2 and of mixtures of CO_2 with CH_4 on the sealing capacity of cap rock at 37°C and 100bar, Chem. Geol. 367 (2014) 39–50.
[17] H. Liu, Z. Hou, P. Were, Y. Gou, L. Xiong, X. Sun, Modelling CO_2-brine-rock interactions in the upper paleozoic formations of ordos basin used for CO_2 sequestration, Environ. Earth Sci. 73 (5) (2015) 2205–2222.
[18] W. van Berk, Y. Fu, H.-M. Schulz, Creation of pre-oil-charging porosity by migration of source-rock-derived corrosive fluids through carbonate reservoirs: one-dimensional reactive mass transport modelling, Pet. Geosci. 21 (2014) 35–42.
[19] T.H. Van Pham, P. Aagaard, H. Hellevang, On the potential for CO_2 mineral storage in continental flood basalts - PHREEQC batch- and 1D diffusion-reaction simulations, Geochem. Trans. 13 (5) (2012).
[20] J.L. Palandri, Y.K. Kharaka, A Compilation of Rate Parameters of Water-mineral Interaction Kinetics for Application to Geochemical Modeling, California, Menlo Park, 2004.
[21] L. Marini, Geological Sequestration of Carbon Dioxide: Thermodynamics, Kinetics, and Reaction Path Modeling, Elsevier, Amsterdam, 2007.
[22] W. Stumm, J.J. Morgan, Aquatic Chemistry: an Introduction Emphasizing Chemical Equilibria in Natural Waters, second ed., John Wiley & Sons, Inc., United States of America, 1981.
[23] H.C. Helgeson, Solution chemistry and metamorphism, Res. Geochem. 2 (1967) 362–404.
[24] H.C. Helgeson, PII: 0016-7037(68)90100-2: evaluation of irreversible reactions in geochemical processes involving minerals and aqueous solutions—I. Thermodynamic relations, Geochim. Cosmochim. Acta 32 (8) (1968) 853–877.
[25] H.C. Helgeson (Ed.), Mass Transfer Among Minerals and Hydrothermal Solutions, second ed., Wiley, New York, 1979.
[26] H.C. Helgeson, R.M. Garrels, F.T. Mackenzie, Evaluation of irreversible reactions in geochemical processes involving minerals and aqueous solutions: II. Applications, Geochim. Cosmochim. Acta 33 (1969) 455–481.
[27] H.C. Helgeson, T.H. Brown, A. Nigrini, T.A. Jones, Calculation of mass transfer in geochemical processes involving aqueous solutions, Geochim. Cosmochim. Acta 34 (1970) 569–592.
[28] A.R. Bowden, A. Rigg, Assessing reservoir performance risks in CO_2 storage projects, Greenh. Gas. Control Technol. 1 (2005) 683–691.
[29] S. Angus, B. Armstrong, K.M. De Reuck, International thermodynamic tables of the fluid state, Carbon Dioxide, Union pure Appl. Chem. 3 (1976).
[30] H. Salimi, K.-H. Wolf, J. Bruining, The influence of capillary pressure on the phase equilibrium of the CO_2–water system: application to carbon sequestration combined with geothermal energy, Int. J. Greenh. Gas Control 11 (2012) S47–S66.
[31] E. Lindenberg, D. Wessel-Berg, Vertical convection in an aquifer column under a gas cap of CO_2, Energy Convers. Manag. 38 (1997) 229–234.
[32] C.A. Rochelle, Y.A. Moore, The Solubility of Supercritical CO_2 into Pure Water and Synthetic Utsira Pore Water: British Geological Survey Report CR/02/052N, 2002.
[33] E.T. Arning, Y. Fu, W. van Berk, H.-M. Schulz, Organic carbon remineralisation and complex, early diagenetic solid–aqueous solution–gas interactions: case study ODP Leg 204, Site 1246 (Hydrate Ridge), Mar. Chem. 126 (1–4) (2011) 120–131.
[34] E.L. Cussler, Diffusion: Mass Transfer in Fluid Systems, third ed., Cambridge Univ. Press, Cambridge, 2009.
[35] S.J. Kemp, J. Bouch, H.A. Murphy, Mineralogical Characterisation of the Nordland Shale, UK Quadrant 16, Northern North Sea, British Geological Survey, Commissioned Report, CR/01/136, 2001.
[36] D.L. Parkhurst, C. Appelo, Description of Input for PHREEQC Version 3—A Computer Program for Speciation, Batch-reaction, One-dimensional Transport, and Inverse Geochemical Calculations: U.S. Geological Survey Techniques and Methods, 2013.
[37] L. De Windt, A. Burnol, P. Montarnal, J. van der Lee, Intercomparison of reactive transport models applied to UO_2 oxidative dissolution and uranium migration, J. Contam. Hydrol. 61 (2003) 303–312.
[38] O. Gundogan, E. Mackay, A. Todd, Comparison of numerical codes for geochemical modelling of CO_2 storage in target sandstone reservoirs, Chem. Eng. Res. Des. 89 (2011) 1805–1816.
[39] B. Nowack, K.U. Mayer, S.E. Oswald, W. van Beinum, C.A.J. Appelo, D. Jacques, P. Seuntjens, F. Gérard, B. Jaillard, A. Schnepf, T. Roose, Verification and intercomparison of reactive transport codes to describe root-uptake, Plant Soil 285 (2006) 305–321.
[40] C. Haase, F. Dethlefsen, M. Ebert, A. Dahmke, Uncertainty in geochemical modelling of CO_2 and calcite dissolution in NaCl solutions due to different modelling codes and thermodynamic databases, Appl. Geochem. 33 (2013) 306–317.
[41] D.L. Parkhurst, C. Appelo, Users Guide to PHREEQC (Version 2)— a Computer Program for Speciation, Batch-reaction, One-dimensional Transport and Inverse Geochemical Calculations, U.S. Geological Survey, Denver, Colorado, 1999.
[42] D. Schäfer, Numerische Modellierung Reaktiver Prozesse Organischer Kontaminanten in Grundwasserleitern: Habilitationsschrift, 2004.
[43] H. Hellevang, P. Aagaard, E.H. Oelkers, B. Kvamme, Can dawsonite permanently trap CO_2? Environ. Sci. Technol. 39 (21) (2005) 8281–8287.
[44] J. Rutqvist, J. Birkholzer, F. Cappa, C.-F. Tsang, Estimating maximum sustainable injection pressure during geological sequestration of CO_2 using coupled fluid flow and geomechanical fault-slip analysis, Energy Convers. Manag. 48 (6) (2007) 1798–1807.
[45] L.F. Konikow, J.D. Bredehoeft, Ground-water models cannot be validated, Adv. Water Resour. 15 (1) (1992) 75–83.
[46] A. Verma, K. Pruess, Thermohydrological conditions and silica redistribution near high-level nuclear wastes emplaced in saturated geological formations, J. Geophys. Res. 93 (1988) 1159–1173.
[47] P.J. Vaughan, Analysis of permeability reduction during flow of heated, aqueous fluid through westerly granite, in: C.-F. Tsang (Ed.), Coupled Processes Associated with Nuclear Waste Repositories, Acad. Pr, Orlando, Fla, 1987, pp. 529–539.
[48] H. Pape, C. Clauser, J. Iffland, Variation of permeability with porosity in sandstone diagenesis interpreted with a fractal pore space model, Pure Appl. Geophys. 157 (4) (2000) 603–619.
[49] M. Fleury, P. Berne, P. Bachaud, Diffusion of dissolved CO_2 in caprock, Energy Procedia 1 (1) (2009) 3461–3468.